Chemical Science

ROYAL SOCIETY OF CHEMISTRY

EDGE ARTICLE

View Article Online
View Journal | View Issue

Cite this: *Chem. Sci.*, 2026, **17**, 6500

All publication charges for this article have been paid for by the Royal Society of Chemistry

Received 4th December 2025
Accepted 31st January 2026

DOI: 10.1039/d5sc09514j

rsc.li/chemical-science

Achieving (quasi)-monocoordination in metal complexes with an exceptionally bulky carbene ligand

Ludwig Zapf * and Eric Rivard *

Bulky *N*-heterocyclic carbenes (NHCs) are powerful tools for controlling the coordination environment and reactivity at inorganic elements. Herein, we report an exceptionally bulky NHC, ^{Bn}ITr (^{Bn}ITr = [(C_6H_4){$NCPh_3$}$_2$C:]), which features a percent buried volume (%V_{bur}) that exceeds 60%. The steric and electronic properties of ^{Bn}ITr were elucidated through a combined experimental and computational study focused on selected silver, gold, and rhodium complexes. The structural impact of the benzylated backbone in ^{Bn}ITr leads to the positioning of phenyl rings within the flanking *N*-trityl (CPh_3, Tr) groups in close proximity to the carbene donor center, enabling the isolation/stabilization of hitherto elusive examples of (quasi)-monocoordinated lithium and gallium(I) cations. Attempts to generate the one-coordinate Pd(0) complex, [^{Bn}ITr–Pd], led to an unusual redox-triggered ligand activation/–CPh_3 group migration to palladium.

Introduction

Modern chemistry benefits from the use of bulky ligands to enforce unusually low coordination environments about an inorganic element, leading to associated breakthroughs in catalysis.[1–3] Over the past few decades *N*-heterocyclic carbenes (NHCs) have emerged as an especially versatile ligand class owing to their tunable σ-donor and π-acceptor properties, high stability, and considerable steric flexibility *via* backbone and *N*-substituent modification.[4–6] NHCs are particularly useful in stabilizing inorganic elements in unusually low oxidation states due a combination of strong carbene-element ligation and/or a controllable increase in ligand bulk.[7–11] Moreover, an ongoing topic of study in coordination chemistry is the design of new exceptionally bulky ligands that enable (quasi)-monocoordinate complex formation. Specifically, a high degree of ligand steric bulk circumvents the formation of multiple strong metal–ligand (M–L) bonds, while also suppressing homoatomic M–M bonding (oligomerization).[12–14]

Earlier work from our group on the design of bulky monodentate ligands led to the synthesis of the *N*-heterocyclic carbene, ITr (**I**, ITr = [$(HCNCPh_3)_2$C:], Fig. 1), featuring a pair of sterically shielding trityl (CPh_3) groups. Notably, ITr is capable of stabilizing low-valent main group element cations, such as $[GeCl]^+$, as well as Ag^+ in the form of a weakly associated dimer $[ITr–Ag]_2$.[15,16]

Continuing on the theme of carbene ligand development, organ and co-workers prepared the bulky NHC DiMeIHept^{Cl} (**II**, Fig. 1)[17–19] and recently observed experimental evidence for transient, monocoordinated complex [NHC–Pd(0)].[14] Also, the Szostak group reported the bulkiest NHC to date, IPr**$^{(4-Bp)}$ (**III**, Fig. 1), with a key structural feature being the placement of sterically shielding biphenyl groups about the imidazole scaffold, leading to a very high reported percent buried volume (%V_{bur})[20,21] of 58.8%.[22]

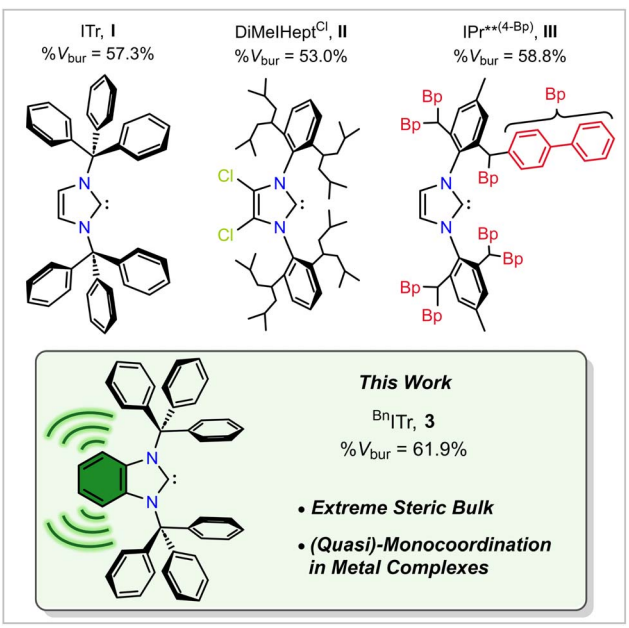

Fig. 1 Selected literature-known sterically encumbered NHCs (I–III, top) and ^{Bn}ITr (3) presented in this study.

Department of Chemistry University of Alberta 11227 Saskatchewan Dr., Edmonton, Alberta T6G 2G2, Canada. E-mail: lzapf@ualberta.ca; erivard@ualberta.ca

In this article, we report the preparation of the exceptionally bulky NHC ligand ^{Bn}ITr (**3**, ^{Bn}ITr = [(C$_6$H$_4$){NCPh$_3$}$_2$C:], Fig. 1) with a percent buried volume that exceeds 60%. Combined experimental and computational studies are used to clarify the steric and electronic features of this new ligand archetype. We also use the unique steric profile of ^{Bn}ITr (**3**) to stabilize Li(I) and Ga(I) cations at the carbene center in a (quasi)-monocoordinated environment and attempt to access a one-coordinate palladium(0) complex.

Results and discussion

The bis(trityl)-functionalized NHC, ^{Bn}ITr (**3**), was readily prepared on a gram-scale in two steps starting from commercially available 2-trityl-benzimidazole (**1**, Scheme 1, for the molecular structure see Fig. S25 in the SI). First, **1** was combined with [Ph$_3$C]OTf (OTf = O$_3$SCF$_3$)[23] in dichloromethane, and the imidazolium salt [^{Bn}ITrH]OTf (**2**, for the molecular structure see Fig. S26 in the SI) was isolated in an excellent yield of 94%. Treating **2** with a stoichiometric amount of KO^{t}Bu in benzene at room temperature resulted in the precipitation of KOTf and the selective formation of target compound ^{Bn}ITr (**3**), which was isolated as a colorless solid in a 93% yield. **3** is stable up to 188 °C in the solid state, and no decomposition was observed in a benzene solution heated to 100 °C (sealed tube). The ^{13}C{^{1}H} spectrum (C$_6$D$_6$ solution) reveals a characteristic resonance at δ 233.2 ppm, which is in the typical range observed for carbene carbon nuclei;[24] *e.g.*, δ 225.8 ppm for **I** (ITr)[15] or δ 224.7 ppm for ^{Bn}I^{t}Bu (^{Bn}I^{t}Bu = [(C$_6$H$_4$){N^{t}Bu}$_2$C:]).[25]

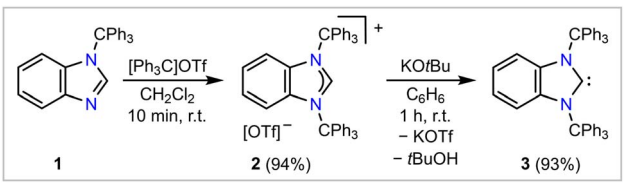

Scheme 1 Synthesis of [^{Bn}ITrH]OTf (**2**) and ^{Bn}ITr (**3**).

Single crystals of **3** suitable for single-crystal X-ray diffraction (SC-XRD) were obtained from a solution of benzene and hexanes (1 : 4) at −35 °C (Fig. 2A).[26] As evident from the molecular structure of **3**, the benzylated backbone creates sufficient steric impact to force a rotation of the trityl groups towards the carbene carbon atom, leading to a highly shielded carbene center. Remarkably, this is not the case when the benzylated backbone is replaced with an unsaturated backbone, as in ITr (**I**, Fig. 2C).[15] Compared to **3**, the trityl groups in **I** are collectively rotated by 180°, creating less steric bulk in ITr: while **I** features an open cone-shaped pocket within the first coordination sphere of the carbene donor center, two opposing phenyl groups of the *N*-bound trityl moieties in **3** minimize the void in proximity to the carbene carbon atom by effectively flanking the ^{carbene}C donor atom (see Fig. 2A–C). Despite these different orientations, the N–C^{CPh3} distances and C^{carbene}–N–C^{CPh3} angles in **I** [1.4912(17) Å; 120.22(12)°; mean values] and **3** [1.503(2) Å; 123.08(13)°; mean values] remain similar.

The structural parameters of **3** and **I** were computed by DFT methods in the gas phase[26] with the resulting optimized molecular structures matching well those derived from SC-XRD. These computations confirm that introduction of the phenylene (C$_6$H$_4$)-unit at the NHC backbone leads to significantly different

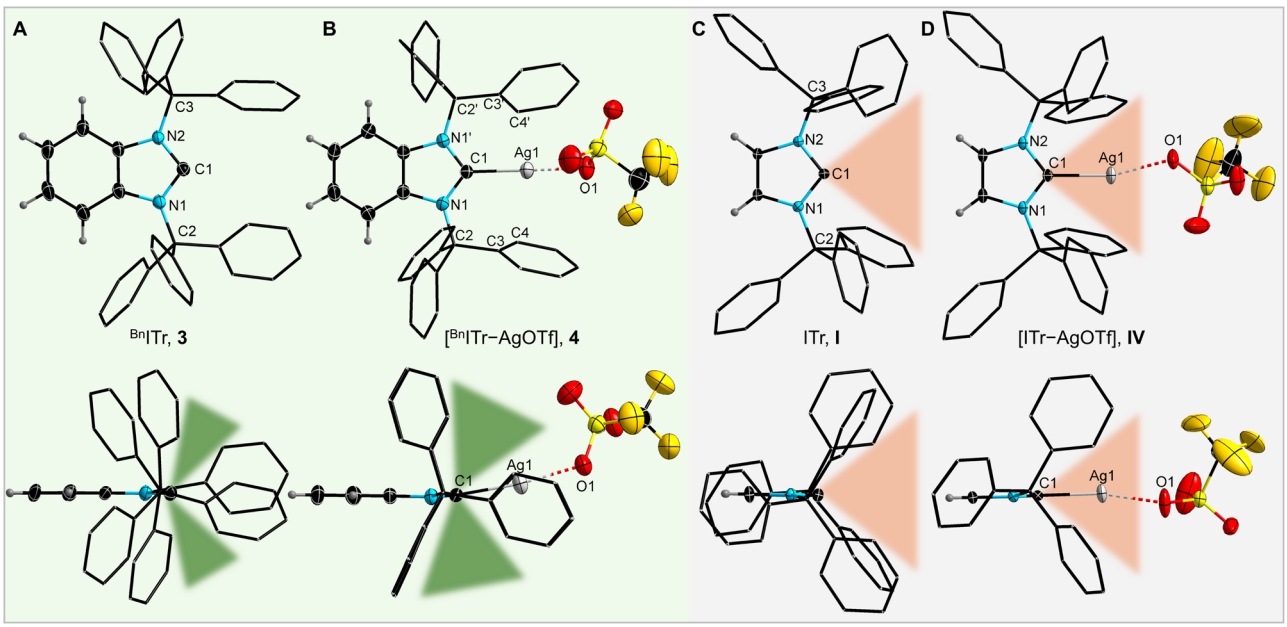

Fig. 2 Two orientations of the molecular structures (ellipsoids are drawn at 50% (**3**, **4**) or 35% (**I**, **IV**) probability level except for the H atoms that are depicted with arbitrary radii; disorder in the [OTf]$^-$ anions (**4**, **IV**), disordered co-crystallized *n*-hexane (**3**), and the H atoms of the CPh$_3$ moieties are omitted for clarity and their C atoms are depicted as wireframe model) of ^{Bn}ITr (**3**, **A**), [^{Bn}ITr–AgOTf] (**4**, **B**), ITr (**I**, **C**), and [ITr–AgOTf] (**IV**, **D**).

steric profiles around the ^{carbene}C atom of the free NHCs ^{Bn}ITr (**3**) and ITr (**I**) owing to the difference in orientation of the flanking trityl groups.

The computed molecular orbitals in **3** (B3LYP/def2-TZVPP level of theory, see Fig. S41)[26] reveal that the C(s)-type σ-donor orbital is the HOMO (−5.49 eV), which is higher in energy compared to those of benchmark carbenes like ^{Bn}IMe (−6.43 eV; ^{Bn}IMe = [(C$_6$H$_4$){NMe}$_2$C:]), IMe (−5.82 eV; IMe = [(HCNMe)$_2$C:]), and **I** (−5.62 eV), suggesting that **3** is the strongest σ-donor in this series. The computed LUMO + 1 (−0.80 eV) and the LUMO + 2 (−0.67 eV) of **3** were identified as low-energy π-accepting C(p)-type orbitals (see Fig. S40 and S41).[26] Therefore, ^{Bn}ITr should also be a potent π-acceptor, as the energies of the abovementioned LUMOs in **3** are lower than the corresponding C(p)-type π-accepting orbitals of IMe (1.00 eV, LUMO + 1), **I** (0.82 eV, LUMO + 12), and even cAAC^{Me} (−0.45 eV, LUMO; cAAC^{Me} = [DippNCMe$_2$CH$_2$CMe$_2$C:], Dipp = 2,6-^{i}Pr$_2$C$_6$H$_3$). Of note, a detailed study on the electronic influence afforded by the benzylation of NHC backbones has been reported recently.[27]

To further probe the steric and electronic properties of ^{Bn}ITr (**3**) experimentally, this bulky carbene was used to generate various metal complexes of silver, gold, and rhodium (Scheme 2). Combining **3** with a stoichiometric amount of AgOTf or AuCl·SMe$_2$ resulted in the formation of [^{Bn}ITr–AgOTf] (**4**) and [^{Bn}ITr–AuCl] (**5**) in 96% and 91% isolated yield, respectively. The molecular structures of **4** and **5** were determined by SC-XRD (Fig. 2B and S29)[26] show that the initial orientation of the trityl groups in free ^{Bn}ITr is preserved upon metal complexation, resulting in a highly shielded metal center in each case. Another notable feature within the structures of **4** and **5** is that the metal atoms are pushed out of the plane formed by the imidazolium carbene ring atoms, resulting in deviation of the NHC(ring centroid)–C1–M (M = Ag, Au) angles from 180° to pitch angles of 170.20(18) and 165.5(2)°, respectively.[26] For comparison, the [ITr–AgOTf] (**IV**)[16] complex of NHC **I** shows a different orientation of the trityl groups (Fig. 2D) with significantly less steric shielding around the metal, as reflected by the difference in the closest Ag···^{Aryl}C distances in **4** [2.870(3) Å] and **IV** [3.095(2) Å]. Furthermore, due to lower steric bulk of ITr (**I**) *vs.* ^{Bn}ITr (**3**), the Ag atom in **IV** remains in the NHC plane [NHC(ring centroid)–C1–Ag = 180.0(4)°]; however, the C1–Ag1 distances in **IV** [2.097(3) Å] and **4** [2.119(4) Å] are similar. The differences in the steric profiles of the two ligands **3** and **I** is also evident from the steric maps calculated from the structural data of **4** and **IV** (Fig. 3) and the significant differences in the estimated total percent buried volumes and the %V_{bur} per quadrant:[20,21,26] ITr **I** features a %V_{bur} of 57.3% for the respective [NHC–AuCl] complex and of 60.4% calculated for the Ag complex **IV**, with values in the quadrants ranging from 52.8 to 68.0%;[15,16] for ^{Bn}ITr **3**, a %V_{bur} of 60.5% was evaluated from the structural data of [^{Bn}ITr–AuCl] (**5**) and a %V_{bur} value of 61.9% from the Ag complex [^{Bn}ITr–AgOTf] (**4**), with values in the quadrants ranging from 49.0 to 74.7%. ^{Bn}ITr **3** is therefore even bulkier than IPr**$^{(4-Bp)}$ **III** (Fig. 1), which was previously the bulkiest NHC ligand reported to date, with a %V_{bur} of 58.8% for the respective [NHC–CuCl] complex and 56.2% for the respective [NHC–AgCl] complex.[22,28]

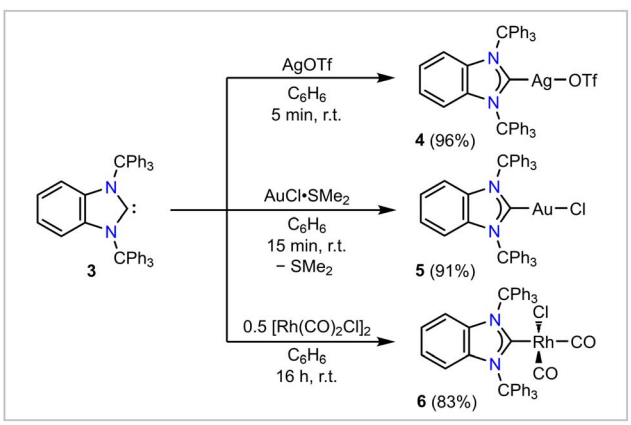

Scheme 2 Synthesis of [^{Bn}ITr–AgOTf] (**4**), [^{Bn}ITr–AuCl] (**5**), and [^{Bn}ITr–Rh(CO)$_2$Cl] (**6**).

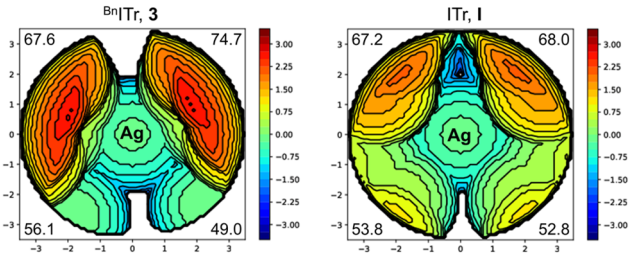

Fig. 3 Steric maps of ^{Bn}ITr, **3**, and ITr, **I**, derived from the structural data of **4** and **IV**, showing %V_{bur} per quadrant.

To experimentally quantify the electronic properties of ^{Bn}ITr (**3**), this carbene was combined with 0.5 eq. of [Rh(CO)$_2$Cl]$_2$, furnishing [^{Bn}ITr–Rh(CO)$_2$Cl] (**6**) as a pale-yellow solid in 83% isolated yield. Two IR ν(CO) stretches were observed at 2068 and 1990 cm^{-1} from a dichloromethane solution of **6**, resulting in a Tolman electronic parameter (TEP)[29,30] of 2043 cm^{-1}. In accordance with the calculated HOMO energy of **3** (*vide supra*), this value implies a remarkable donor strength that exceeds that of benchmark NHCs like IMe (TEP = 2050 cm^{-1})[31] and IPr (TEP = 2052 cm^{-1}, IPr = [(HCNDipp)$_2$C:]).[29]

Motivated by the excellent donor ability and the steric encumbering nature of **3**, we targeted the synthesis of a (quasi)-monocoordinated palladium(0) complex, [NHC–Pd(0)]. Such a species is often postulated to be a key intermediate for palladium-catalyzed cross-coupling reactions, but has never been isolated.[14] In pursuit of this goal, compound **3** was mixed with 0.5 eq. of [Pd(π-cin)Cl]$_2$ (cin = cinnamyl, PhC$_3$H$_4$), yielding [^{Bn}ITr–Pd(π-cin)Cl] (**7**) as a pale-yellow solid in 98% isolated yield (Scheme 3). The molecular structure of **7** (Fig. 4) obtained by SC-XRD reveals typical C1–Pd1 [2.032(4) Å] and Pd1–Cl1 [2.391(1) Å] bond lengths; for comparison, the corresponding ^{NHC}C–Pd and Pd–Cl distances in [**II**–Pd(π-cin)Cl] are 2.074(2) Å and 2.372(1) Å, respectively.[18]

Treating **7** with one equivalent of KO^{t}Bu resulted in a rapid reaction accompanied by the precipitation of a fine white solid

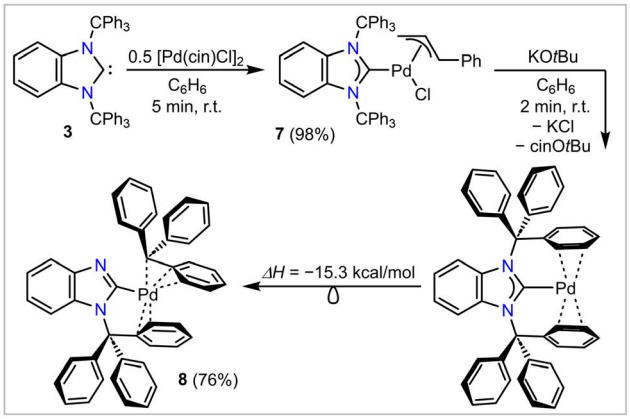

Scheme 3 Synthesis of [^{Bn}ITr–Pd(π-cin)Cl] (**7**, cin = cinnamyl) and reaction of **7** with KO^{t}Bu to yield [^{Bn}ImTr–Pd–Tr] (**8**) *via* migration of a trityl group within the proposed intermediate [^{Bn}ITr–Pd].

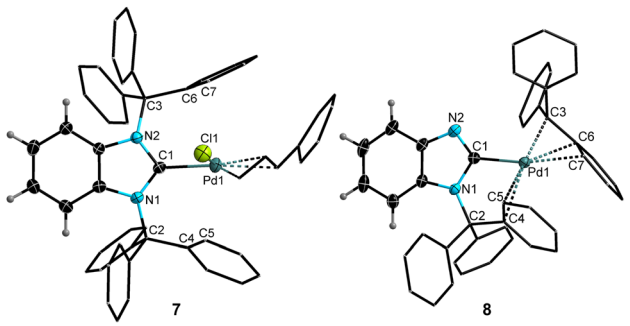

Fig. 4 Molecular structures of **7** and **8** (ellipsoids are drawn at 35% probability level except for the H atoms that are depicted with arbitrary radii; the H atoms of the CPh_3 moieties and the cinnamyl moiety (**7**) are omitted for clarity, and their C atoms are depicted as wireframe model). Selected bond lengths [Å] and angles [°]: **7**: N1–C1 1.365(5), C1–N2 1.368(5), N1–C2 1.513(5), N2–C3 1.516(5), C1–Pd1 2.032(4), Pd1–Cl1 2.3914(11), C4–Pd1 3.131(4), C5–Pd1 2.947(4), C6–Pd1 3.120(4), C7–Pd1 3.031(4); N1–C1–N2 106.1(3), C1–N1–C2 128.0(3), C1–N2–C3 130.1(3); **8**: N1–C1 1.403(9), C1–N2 1.327(9), N1–C2 1.476(8), C1–Pd1 2.005(7), C4–Pd1 2.435(6), C5–Pd1 2.367(7), C3–Pd1 2.113(8), C6–Pd1 2.246(8), C7–Pd1 2.345(7); N1–C1–N2 111.0(6), C1–N1–C2 124.3(5), α = 168.56(15).

(presumably KCl) and a color change of the reaction solution from pale-yellow to dark-orange. *In situ* ^{1}H NMR spectroscopy showed the formation of the expected cinnamyl-butoxy elimination product cin–O^{t}Bu, and generation of a new carbene-containing product that was highly unstable in solution (full decomposition within *ca.* 90 min., at room temperature). Rapid precipitation of this new carbene-containing species from the reaction mixture by adding hexanes allowed its isolation and characterization as a bright-yellow solid in 76% yield. To our surprise, the molecular structure derived by SC-XRD (Fig. 4) revealed that this compound was not the expected one-coordinated [^{Bn}ITr–Pd] complex. Instead, one of the N–C^{CPh3} bonds was cleaved and the trityl group migrated to the Pd center, resulting in the η^3-benzylic coordinated compound [^{Bn}ImTr–Pd–Tr] (**8**, Scheme 3). The η^3-coordination mode of the migrated trityl moiety [C–Pd distances of 2.113(8) to 2.345(7) Å], is reminiscent to what is found within the known complex [(acac)Pd–Tr] (acac = pentane-2,4-dionate) with Pd–C contacts ranging from 2.105(6) Å to 2.200(7) Å.[32,33] Quantum chemical calculations[26] confirmed that the migration of one of the trityl groups from the proposed *in situ* generated complex [^{Bn}ITr–Pd] to yield **8** is exergonic (ΔG) by −15.3 kcal mol^{-1} (Scheme 3).

Attempts to trap the (quasi)-monocoordinated species [^{Bn}ITr–Pd] at low temperatures or in the presence of CO, PMe_3, diphenylacetylene, $B(C_6F_5)_3$, or $Fe(CO)_5$ were unsuccessful, and resulted in intractable product mixtures. The computed structure of [^{Bn}ITr–Pd] (B3LYP/def2-TZVPP level of theory, see Fig. S46)[26] lies in an energetic minimum and features a ^{carbene}C–Pd bond length of 2.122 Å. The orientation of the trityl groups is similar to that in the above mentioned ^{Bn}ITr metal complexes **4**–**7** with ^{Aryl}C···Pd distances in the range of 2.157–2.822 Å. The calculated HOMO energy in [^{Bn}ITr–Pd] (−4.04 eV) is significantly higher compared to that calculated for rearrangement product **8** (−6.21 eV) while the HOMO–LUMO gap in [^{Bn}ITr–Pd] (ΔE = 3.02 eV) is significantly smaller compared to **8** (ΔE = 4.63 eV).

Next, we turned our attention to the isolation of hitherto elusive examples of (quasi)-monocoordinated complexes of main group cations supported by ^{Bn}ITr. To achieve this goal and minimize cation–anion interactions, we opted to react **3** with salts containing Krossing's weakly coordinating anion [Al(OR^F)$_4$]$^-$ (R^F = C(CF$_3$)$_3$).[34] Upon treatment of **3** with Li[Al(OR^F)$_4$],[34] the target complex [^{Bn}ITr–Li][Al(OR^F)$_4$] (**9**) was obtained as a white solid in a 96% yield (Scheme 4). Crystallization of **9** from a 5 : 1 mixture of fluorobenzene and benzene at −35 °C furnished colorless single crystals suitable for SC-XRD. The refined molecular structure of **9** (Fig. 5) matches closely with the DFT-optimized[26] structure of the [^{Bn}ITr–Li]$^+$ cation in the gas phase; specifically, shielding of the lithium cation by the flanking aryl group interactions results in an unprecedented (quasi)-monocoordinated Li$^+$ center. The experimental [2.092(6) Å] and calculated [2.060 Å] C1–Li distance is on the lower end of the typical range reported for ^{carbene}C–Li bond lengths:[35] *e.g.*, 2.155(4) Å for [I^{t}Bu–Li(η^5-1,2,4-(Me$_3$Si)$_3$C$_5$H$_2$)] (I^{t}Bu = [(HCN^{t}Bu)$_2$C:]).[36] The closest Li···^{Aryl}C distances in **9** [C5–Li1 = 2.426(5) Å and C8–Li1 = 2.440(8) Å] are consistent with the Atoms-in-Molecules (AIM)-calculated bond critical points and paths (Fig. 5) and very low Wiberg bond indices of 0.011 involving the Li1···C5 and Li1···C8 contacts. For comparison, the closest Li···C^{Aryl} distances in the bis(η^6-benzene)lithium cation, reported by Erker and co-workers, are 2.404(7) Å.[37] In contrast to previously known carbene–lithium

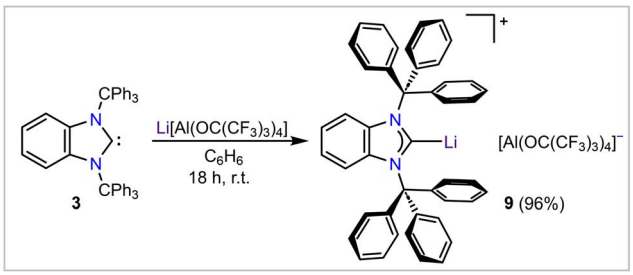

Scheme 4 Synthesis of [^{Bn}ITr–Li][Al(OR^F)$_4$] (**9**).

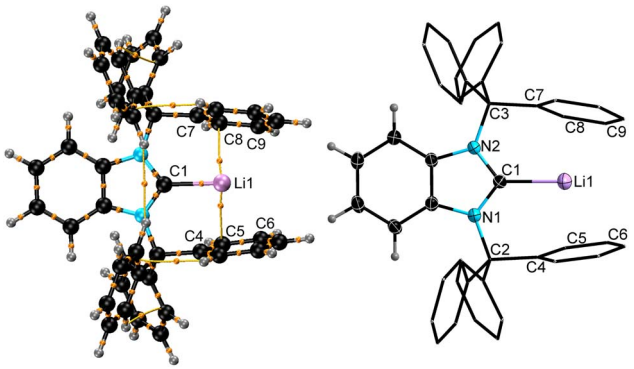

Fig. 5 Computed structure including bond critical points and paths (left) and molecular structure of **9** derived by SC-XRD (right, ellipsoids are drawn at 35% probability level except for the H atoms that are depicted with arbitrary radii; the $[Al(OC(CF_3)_3)_4]^-$ anion and the H atoms of the CPh_3 moieties are omitted for clarity and their C atoms are depicted as wireframe model). Selected bond lengths [Å] and angles [°]: N1–C1 1.355(3), C1–N2 1.359(4), N1–C2 1.496(4), N2–C3 1.496(3), C1–Li1 2.092(6), C4–Li1 2.559(6), C5–Li1 2.426(5), C6–Li1 2.571(5), C7–Li1 2.572(6), C8–Li1 2.440(8), C9–Li1 2.522(7); N1–C1–N2 105.3(2), C1–N1–C2 123.2(2), C1–N2–C3 123.4(2).

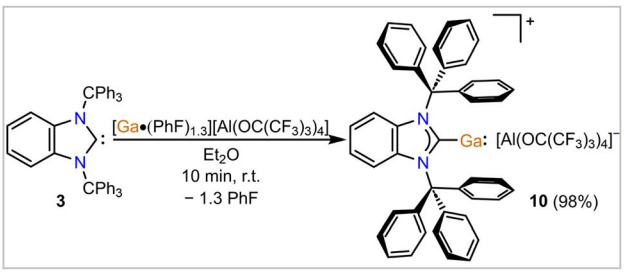

Scheme 5 Synthesis of $[^{Bn}ITr–Ga][Al(OR^F)_4]$ (**10**).

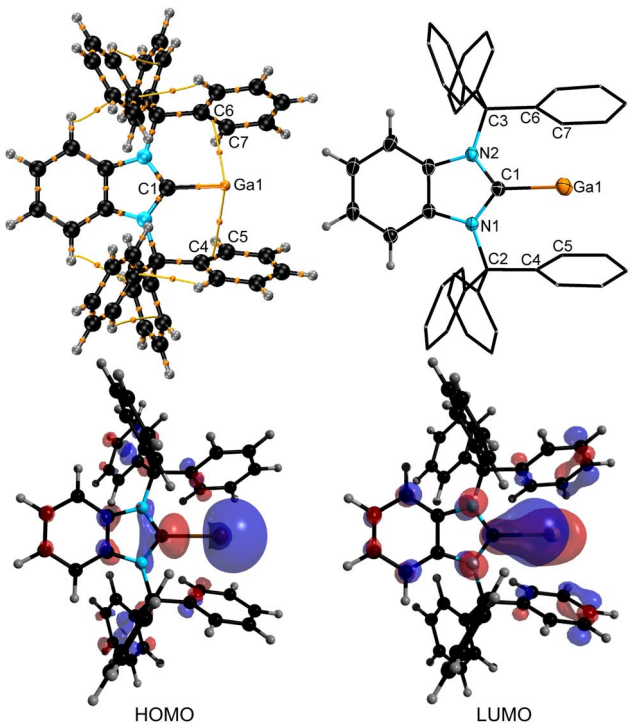

Fig. 6 Computed structure including bond critical points and paths (top left), selected computed molecular orbitals (bottom), and molecular structure of **10** derived by SC-XRD (top right, ellipsoids are drawn at 35% probability level except for the H atoms that are depicted with arbitrary radii; the $[Al(OC(CF_3)_3)_4]^-$ anion and the H atoms of the CPh_3 moieties are omitted for clarity and their C atoms are depicted as wireframe model). Selected bond lengths [Å] and angles [°]: N1–C1 1.367(6), C1–N2 1.353(6), N1–C2 1.496(6), N2–C3 1.497(6), C1–Ga1 2.284(5), C4–Ga1 2.848(5), C5–Ga1 2.850(6), C6–Ga1 2.803(4), C7–Ga1 2.791(4); N1–C1–N2 106.0(4), C1–N1–C2 124.8(4), C1–N2–C3 125.4(4).

complexes,[35] **9** is the first example of a molecular monomeric complex bearing no extra ligand(s) or solvent(s) at the lithium center.

Finally, we targeted the stabilization of a (quasi)-monocoordinated low-oxidation state main group metal and focused on the Ga(I) cation as a proof of concept. It should be stated that Power and co-workers did prepare a one-coordinate Ga(I) compound, $^{iPr6}Ar–Ga$: (^{iPr6}Ar = 2,6-$Trip_2$-3,5-$^iPr_2C_6H$; Trip = 2,4,6-$^iPr_3C_6H_2$), using a very bulky anionic terphenyl ligand.[38] Krossing and co-workers have prepared a variety of Ga(I) complexes of the general formula $[GaL_n][Al(OR^F)_4]$ with a variety of ligands (L_n), including arenes, amines, and phosphines, and used the resulting subvalent gallium cations in catalytically relevant bond activation processes.[39–45] Interestingly, reactions of $[Ga(PhF)_{2–3}][Al(OR^F)_4]$ with the bulky carbene donors IPr and IMes (IMes = [(HCNMes)$_2$C:], Mes = 2,4,6-$Me_3C_6H_2$) resulted in *bis*-NHC complexes $[Ga(NHC)_2][Al(OR^F)_4]$ with bent [NHC–Ga–NHC]$^+$ cations.[46] Given that ^{Bn}ITr (**3**) provides more steric shielding and is a stronger σ-donor compared to the aforementioned NHCs (*vide supra*), we were eager to find out if our new NHC is capable of yielding an elusive mono-substituted cationic [NHC–Ga(I)]$^+$ complex. As hoped, reactions of stoichiometric amounts of $[Ga(PhF)_{1.3}][Al(OR^F)_4]$ and **3** resulted in the clean formation of the target compound $[^{Bn}ITr–Ga][Al(OR^F)_4]$ (**10**, Scheme 5).

The molecular structure derived by SC-XRD confirms the (quasi)-monocoordination of the Ga(I) cation by the ^{Bn}ITr ligand with overall metric parameters that match those derived by DFT computations in the gas phase (Fig. 6). The Ga1–C1 bond length in **10** of 2.284(5) Å (DFT calc. value of 2.283 Å) is in range of the mean Ga–^{NHC}C bond lengths (2.288(3) Å) reported for $[Ga(IPr)_2]^+$.[46] The Ga(I) cation in 10 features some weak bonding interactions with the flanking aryl moieties of the ^{Bn}ITr ligand, as indicated by AIM bond critical points and -paths located between Ga1 and C4–C5 and C6–C7 (Fig. 6) as well as computed WBI values of 0.033 (Ga1···C4, Ga1···C6) and 0.045 (Ga1···C6, Ga1···C7).[26] The closest Ga···^{Aryl}C contact in the molecular structure of **10** derived by SC-XRD is 2.791(4) Å. Similar to the molecular structures of the ^{Bn}ITr-bound transition metal complexes **4** and **5** (*vide supra*), the Ga atom in 10 is pushed out of the NHC plane, resulting in a NHC–C1–Ga pitch angle of 155.6(2)° [DFT calc. value of 159.2°]. For comparison, the Ga atom was found to be in plane with the small NHC ligand ^{Me}IMe (^{Me}IMe = [(MeCNMe)$_2$C:]) within the DFT-optimized structure

of the hypothetical cation $[^{Me}IMe–Ga]^+$.[46] The frontier orbitals of **10** were computed by DFT calculations and the HOMO and LUMO are shown in Fig. 6. The HOMO consists mainly of the s-orbital at gallium, while the LUMO is a gallium p-orbital that shows some added Ga–C π-interaction with the carbene carbon atom. The position, shape, and ambiphilic nature of these frontier orbitals, in addition to the open coordination site at Ga(I) opposite to the ^{Bn}ITr ligand, makes **10** a promising compound for small molecule activation, which we are planning to investigate closely in the future.

Conclusions

In conclusion, a new highly sterically encumbering NHC ligand, ^{Bn}ITr (**3**), featuring *N*-bound trityl groups and a benzylated backbone has been synthesized. Compared to our previously described ligand ITr (**I**),[15] the phenylene (C_6H_4) backbone in **3** forces a rotation in the trityl group yielding a carbene center that is flanked by two sterically shielding aryl rings. Analysis of the percent buried volume (%V_{bur}) and structural features of the ^{Bn}ITr-coordinated silver and gold complexes **4** and **5** reveal a unique steric profile associated with **3,** which is, to the best of our knowledge, the bulkiest NHC ligand reported to date. Furthermore, quantum chemical calculations and experimental evaluation of the TEP from the rhodium carbonyl complex **6**, reveals ^{Bn}ITr (**3**) is a potent σ-donor and π-acceptor. Pursuit of the (quasi)-monocoordinate palladium complex, [^{Bn}ITr–Pd], led to an unusual trityl group (–CPh_3) migration from the carbene ligand to Pd, affording the η^3-CPh_3 coordinated Pd(II) complex **8**. Nevertheless, **3** proved to be a suitable ligand for the stabilization of main group metal cations [Li(I) and Ga(I)] that approach the unusual coordination number of 1. Future work will target the development of new ^{Bn}ITr complexes as active catalysts with related (quasi)-monocoordinate metal centers as highlighted in this study.

Author contributions

E. R. and L. Z. conceived the project. L. Z. performed the experiments and quantum chemical calculations. L. Z. and E. R. wrote the manuscript.

Conflicts of interest

There are no conflicts to declare.

Data availability

CCDC 2505690 (**8**), 2505691 (**4**), 2505692 (**1**), 2505693 (**2**), 2505694 (**6**), 2505695 (**5**), 2505696 (**10**), 2505697 (**9**), 2505698 (**7**) and 2505699 (**3**) contain the supplementary crystallographic data for this paper.[47a–j]

Supplementary information (SI): experimental details, NMR and IR spectra, details on DFT calculations, and Cartesian coordinates of the DFT optimized structures. See DOI: https://doi.org/10.1039/d5sc09514j.

Acknowledgements

L.Z. thanks the Alexander von Humboldt Foundation for generous support (Feodor Lynen Postdoctoral Research Fellowship). The authors also thank Digital Alliance Canada for computing services. E.R. thanks NSERC of Canada (Discovery Grant: RGPIN-2025-04321) and the Canada Foundation for Innovation for funding.

Notes and references

1 L. J. Taylor and D. L. Kays, *Dalton Trans.*, 2019, **48**, 12365–12381.
2 M. R. Elsby and R. T. Baker, *Chem. Soc. Rev.*, 2020, **49**, 8933–8987.
3 M. Asay, C. Jones and M. Driess, *Chem. Rev.*, 2011, **111**, 354–396.
4 P. Bellotti, M. Koy, M. N. Hopkinson and F. Glorius, *Nat. Rev. Chem.*, 2021, **5**, 711–725.
5 F. Nahra, D. J. Nelson and S. P. Nolan, *Trends Chem.*, 2020, **2**, 1096–1113.
6 V. V. Nesterov, D. Reiter, P. Bag, P. Frisch, R. Holzner, A. Porzelt and S. Inoue, *Chem. Rev.*, 2018, **118**, 9678–9842.
7 E. Peris, *Chem. Rev.*, 2018, **118**, 9988–10031.
8 C. Valente, S. Çalimsiz, K. H. Hoi, D. Mallik, M. Sayah and M. G. Organ, *Angew. Chem., Int. Ed.*, 2012, **51**, 3314–3332.
9 P. P. Nair, A. Jayaraj and C. A. Swamy P, *ChemistrySelect*, 2022, **7**, e202103517.
10 G. G. Zámbó, J. F. Schlagintweit, R. M. Reich and F. E. Kühn, *Catal. Sci. Technol.*, 2022, **12**, 4940–4961.
11 Q. Zhao, G. Meng, S. P. Nolan and M. Szostak, *Chem. Rev.*, 2020, **120**, 1981–2048.
12 M. Dudev, J. Wang, T. Dudev and C. Lim, *J. Phys. Chem. B*, 2006, **110**, 1889–1895.
13 G. Kuppuraj, M. Dudev and C. Lim, *J. Phys. Chem. B*, 2009, **113**, 2952–2960.
14 V. Semeniuchenko, S. Sharif, N. Rana, N. Chandrasoma, W. M. Braje, R. T. Baker, J. M. Manthorpe, W. J. Pietro and M. G. Organ, *J. Am. Chem. Soc.*, 2024, **146**, 29224–29236.
15 M. M. D. Roy, P. A. Lummis, M. J. Ferguson, R. McDonald and E. Rivard, *Chem. Eur J.*, 2017, **23**, 11249–11252.
16 M. M. D. Roy, M. J. Ferguson, R. McDonald and E. Rivard, *Chem. Commun.*, 2018, **54**, 483–486.
17 C. Lombardi, J. Day, N. Chandrasoma, D. Mitchell, M. J. Rodriguez, J. L. Farmer and M. G. Organ, *Organometallics*, 2017, **36**, 251–254.
18 V. Semeniuchenko, S. Sharif, J. Day, N. Chandrasoma, W. J. Pietro, J. Manthorpe, W. M. Braje and M. G. Organ, *J. Org. Chem.*, 2021, **86**, 10343–10359.
19 For details on the determination of the %Vbur of II see the Electronic Supporting Information.
20 A. Gómez-Suárez, D. J. Nelson and S. P. Nolan, *Chem. Commun.*, 2017, **53**, 2650–2660.
21 H. Clavier and S. P. Nolan, *Chem. Commun.*, 2010, **46**, 841–861.
22 Y. Sha, W. Chu, R. Lalancette, R. Szostak and M. Szostak, *Organometallics*, 2025, **44**, 1848–1853.

23 D. A. Straus, C. Zhang and T. D. Tilley, *J. Organomet. Chem.*, 1989, **369**, C13–C17.
24 D. Tapu, D. A. Dixon and C. Roe, *Chem. Rev.*, 2009, **109**, 3385–3407.
25 D. M. Khramov and C. W. Bielawski, *J. Org. Chem.*, 2007, **72**, 9407–9417.
26 For added experimental, crystallographic, and computational details, please see the Electronic Supporting Information.
27 M. S. Luff, C. S. Corsei and U. Radius, *Organometallics*, 2025, **44**, 691–703.
28 Note that the comparability of $\%V_{bur}$ for **3** and **IV** is slightly complicated by the differences in the co-ligand X in the complexes [^{Bn}ITr–AgX] (X = OTf) and [IPr**$^{(4\text{-Bp})}$–AgX] (X = Cl). However, relative to the significant difference in $\%V_{bur}$ of 5.7%, the influence of X is negligible as the coordination number (C.N. = 2) and the coordination mode (linear) of the silver atom are identical in both complexes, the co-ligands do not exhibit interactions with the NHC periphery and are far away from the carbene center (>4.2 Å), and the co-ligands are omitted during the determination of $\%V_{bur}$ in any case.
29 T. Dröge and F. Glorius, *Angew. Chem., Int. Ed.*, 2010, **49**, 6940–6952.
30 C. A. Tolman, *Chem. Rev.*, 1977, **77**, 313–348.
31 L. Zapf, S. Peters, R. Bertermann, U. Radius and M. Finze, *Chem. Eur J.*, 2022, **28**, e202200275.
32 A. Sonada, B. E. Mann and P. M. Maitlis, *J. Chem. Soc., Chem. Commun.*, 1975, 108–109.
33 A. Sonoda, P. M. Bailey and P. M. Maitlis, *J. Chem. Soc., Dalton Trans.*, 1979, 346–350.
34 I. Krossing, *Chem. Eur J.*, 2001, **7**, 490–502.
35 S. Bellemin-Laponnaz and S. Dagorne, *Chem. Rev.*, 2014, **114**, 8747–8774.
36 A. J. Arduengo, M. Tamm, J. C. Calabrese, F. Davidson and W. J. Marshall, *Chem. Lett.*, 1999, **28**, 1021–1022.
37 X. Jie, J. Li, C. G. Daniliuc, A.-L. Wübker, M. R. Hansen, H. Eckert, C. Mück-Lichtenfeld, G. Kehr and G. Erker, *Angew. Chem., Int. Ed.*, 2021, **60**, 22879–22884.
38 Z. Zhu, R. C. Fischer, B. D. Ellis, E. Rivard, W. A. Merrill, M. M. Olmstead, P. P. Power, J. D. Guo, S. Nagase and L. Pu, *Chem. Eur J.*, 2009, **15**, 5263–5272.
39 P. Dabringhaus, A. Barthélemy and I. Krossing, *Z. Anorg. Allg. Chem.*, 2021, **647**, 1660–1673.
40 J. M. Slattery, A. Higelin, T. Bayer and I. Krossing, *Angew. Chem., Int. Ed.*, 2010, **49**, 3228–3231.
41 A. Higelin, U. Sachs, S. Keller and I. Krossing, *Chem. Eur J.*, 2012, **18**, 10029–10034.
42 M. R. Lichtenthaler, A. Higelin, A. Kraft, S. Hughes, A. Steffani, D. A. Plattner, J. M. Slattery and I. Krossing, *Organometallics*, 2013, **32**, 6725–6735.
43 A. Barthélemy, K. Glootz, H. Scherer, A. Hanske and I. Krossing, *Chem. Sci.*, 2022, **13**, 439–453.
44 A. Barthélemy, H. Scherer, M. Daub, A. Bugnet and I. Krossing, *Angew. Chem., Int. Ed.*, 2023, **62**, e202311648.
45 P. Dabringhaus, H. Scherer and I. Krossing, *Nat. Synth.*, 2024, **3**, 732–743.
46 A. Higelin, S. Keller, C. Göhringer, C. Jones and I. Krossing, *Angew. Chem., Int. Ed.*, 2013, **52**, 4941–4944.
47 (*a*) CCDC 2505690: Experimental Crystal Structure Determination, 2026, DOI: 10.5517/ccdc.csd.cc2q3cqy; (*b*) CCDC 2505691: Experimental Crystal Structure Determination, 2026, DOI: 10.5517/ccdc.csd.cc2q3crz; (*c*) CCDC 2505692: Experimental Crystal Structure Determination, 2026, DOI: 10.5517/ccdc.csd.cc2q3cs0; (*d*) CCDC 2505693: Experimental Crystal Structure Determination, 2026, DOI: 10.5517/ccdc.csd.cc2q3ct1; (*e*) CCDC 2505694: Experimental Crystal Structure Determination, 2026, DOI: 10.5517/ccdc.csd.cc2q3cv2; (*f*) CCDC 2505695: Experimental Crystal Structure Determination, 2026, DOI: 10.5517/ccdc.csd.cc2q3cw3; (*g*) CCDC 2505696: Experimental Crystal Structure Determination, 2026, DOI: 10.5517/ccdc.csd.cc2q3cx4; (*h*) CCDC 2505697: Experimental Crystal Structure Determination, 2026, DOI: 10.5517/ccdc.csd.cc2q3cy5; (*i*) CCDC 2505698: Experimental Crystal Structure Determination, 2026, DOI: 10.5517/ccdc.csd.cc2q3cz6; (*j*) CCDC 2505699: Experimental Crystal Structure Determination, 2026, DOI: 10.5517/ccdc.csd.cc2q3d08.